Adsorptive removal of anionic dyes from aqueous solutions using microgel based on nanocellulose and polyvinylamine

Liqiang Jin [a,*], Qiucun Sun [b], Qinghua Xu [b], Yongjian Xu [c]

[a] School of Chemistry and Pharmaceutical Engineering, Qilu University of Technology, Jinan 250353, China
[b] Key Laboratory of Paper Science & Technology of Ministry of Education, Qilu University of Technology, Jinan 250353, China
[c] Shaanxi Province Key Lab of Paper Technology and Specialty Paper, Shaanxi University of Science and Technology, Xi'an 710021, China

HIGHLIGHTS

- A novel microgel was fabricated via nanocellulose and amphoteric polyvinylamine.
- It demonstrated highest dye removal efficiency at acidic pH.
- The sorption kinetic follows pseudo-second-order model.
- The experimental data fit well with Sips isotherm.
- The microgel was an excellent adsorbent for the removal of anionic dyes.

GRAPHICAL ABSTRACT
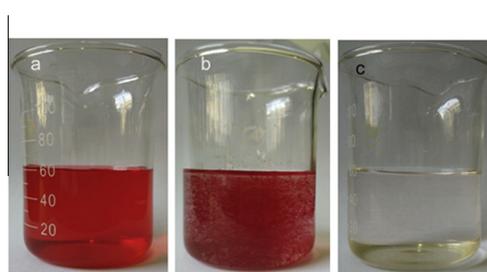
a, before adsorption; b, dye adsorption after 120min; c, after dye removal
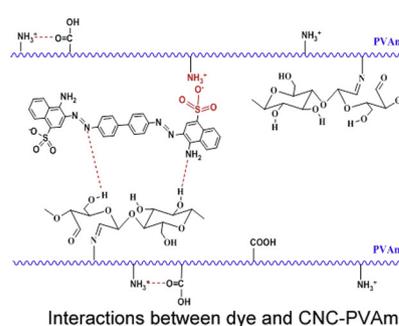
Interactions between dye and CNC-PVAm

ABSTRACT

A novel nanocomposite microgel based on nanocellulose and amphoteric polyvinylamine (PVAm) was fabricated via a two-step method. Firstly, cellulose nanocrystal was oxidized by sodium periodate to yield dialdehyde nanocellulose (DANC). DANC was then used as a crosslinker to react with PVAm to obtain a pH responsive microgel with high density of free amine groups. The microgel was characterized using FTIR, XRD, AFM and elemental analysis. AFM images revealed that the nanocomposite was microspherical particles with a diameter ranging from 200 to 300 nm. The microgel was found to be effective in anionic dye removal at acidic conditions. The adsorption isotherms for congo red 4BS, acid red GR and reactive light yellow K-4G fit well with the Sips model, and the maximum adsorption capacities were 869.1 mg g^{-1}, 1469.7 mg g^{-1} and 1250.9 mg g^{-1}, respectively. The adsorption for these three anionic dyes all followed pseudo second order kinetics, indicating a chemisorption nature.

© 2015 Elsevier Ltd. All rights reserved.

1. Introduction

Dyes are widely used in industries such as textiles, leather, paper, printing, plastics, food, cosmetic, etc. Approximately 15% of the dyes remain as industrial waste and are discharged into water bodies (Kayranli, 2011). Their discharges into hydrosphere have posed serious environmental problems due to their recalcitrant nature. Dyes are usually non-biodegradable and stable to light, heat and oxidizing agents (Wang et al., 2006), hence, physical methods, especially sorption of synthetic dyes on inexpensive and efficient solid supports have been considered a simple and economical process for the removal of dyes from wastewater (Bonetto et al., 2015).

The adsorbents used in water treatment include activated carbons, agricultural solid wastes, industrial by-products, clay minerals, biomass and polymeric resins, etc. (Unuabonah and Taubert, 2014; Yagub et al., 2014). However, conventional adsorbents are

---

* Corresponding author. Tel.: +86 531 89631168; fax: +86 531 89631161.
E-mail address: jlq@qlu.edu.cn (L. Jin).

usually limited by the lack of selectivity and lower adsorption kinetics due to the limited surface area or active sites (Qu et al., 2013). A large surface area and the abundance of adsorption sites are essential for adsorption and removal of contaminants from wastewater (Liu et al., 2014). Nanomaterials, due to their higher surface area and greater number of active sites for interaction with pollutants, are increasingly used in dye removal (Savage and Diallo, 2005). Nanocellulose, extracted from lignocellulosic materials, has attracted increasing attention from many diverse areas due to its unique properties such as high aspect ratio, large specific surface area, good biocompatibility and chemical accessibility. Its high surface area can provide many more active sites on the surface, resulting in high adsorption capability. Zhou et al. (2014) reported a series of partially hydrolyzed polyacrylamide/cellulose nanocrystal (HPAM/CNC) nanocomposite hydrogels with various amounts of CNCs, which were used to remove methylene blue (MB) dye from an aqueous solution. The maximum dye adsorption capacity of HPAM/CNC nanocomposite hydrogels can be improved by the incorporation of CNCs. Maatar et al. (2013) prepared a highly porous organogel from cellulose nanofibrils hydrogel and investigated its adsorption properties towards a wide range of organic solutes. It was shown that by functionalizing the native cellulose nanofibrils of the organogel with hydrophobic hydrocarbon chains, the adsorption capacity of the material is meaningfully boosted.

The adsorbability of biosorbents can be further increased by appropriate functionalization (Ong et al., 2007). Recently, amino-functionalized nanocellulose showed an outstanding adsorption capability for heavy metal ions and anionic dyes, since amino groups are easily protonated under acidic conditions. Jebali et al. (2015) evaluated the adsorption of humic acid by nanocellulose modified with N-(2-aminoethyl)-3-aminopropylmethyldimethoxy silane. It was found that amine-modified nanocellulose could be used for removal of humic acid from wastewater. Hokkanen et al. (2014a) investigated the adsorption properties of aminopropyltriethoxysilane (APS) modified microfibrillated cellulose (MFC) in aqueous solutions containing Ni(II), Cu(II) and Cd(II) ions. The results showed that the modified MFC was very effective for Ni(II), Cu(II) and Cd(II) removal from contaminated water. In our previous work (Jin et al., 2015), cellulose nanocrystal was oxidized by sodium periodate and then grafted with ethylenediamine to obtain amino-functionalized nanocellulose with free primary amino groups. The modified nanocellulose was effective in removal for anionic dyes. Nevertheless, most of the researches are dealing with nanocellulose modified using low molecular weight amines. To our knowledge, nanocellulose modified with polyamine, which was applied in contaminant removal, are not reported.

Polyvinylamine is a potent tool for the modification of macroscopic and nanoparticle surfaces due to its high primary amine groups content (Pelton, 2014). It adsorbs spontaneously and irreversibly on most surfaces in water, generating cationic interfaces. Polyvinylamine could be applied in separation membranes, flocculation, chromatography stationary phases, encapsulation, oil recovery and gene delivery. It is expected that the adsorbability of nanocellulose modified with polyvinylamine would be boosted due to its high content of amine groups.

In this work, a pH responsive nanocomposite microgel based on cellulose nanocrystal and amphoteric PVAm was prepared and applied in dye removal. Firstly, cellulose nanocrystals (CNCs), extracted from bleached kraft pulp, were oxidized by sodium periodate to yield dialdehyde nanocellulose (DANC). DANC was then used as a crosslinker to react with PVAm through a Schiff-base reaction to obtain the nanocomposite microgel (CNC–PVAm). Properties of the microgel were characterized by FTIR, XRD, AFM and elemental analysis. Furthermore, its adsorption capacity for anionic dyes was evaluated.

2. Methods

2.1. Materials

Fully bleached aspen kraft pulp, as an original material used for preparation of the nanocrystalline cellulose, was provided by the Silver Star Paper Co., Ltd, Jinan, China. Amphoteric polyvinylamine with carboxyl as the anionic groups and a molecular weight of 150 kDa was provided by BASF (China) Co. Ltd. Sodium periodate was purchased from Sigma–Aldrich Co. Ltd. The commercial anionic dyes, acid red GR (acid dye), congo red 4BS (direct dye), and reactive light yellow K-4G (reactive dye) were supplied by Tianjin Ruiji Chemical Co. Ltd. Their chemical structure and characteristics are shown in Table 1.

2.2. Preparation of CNC and DANC

CNC was prepared by sulfuric acid hydrolysis of fully bleached kraft pulp and then periodate oxidized to obtain DANC according to the method by Jin et al. (2015). 9 mmol sodium periodate per gram of cellulose nanocrystal was used. The aldehyde group content was determined by the Schiff base reaction between aldehyde groups and hydroxylamine hydrochloride. It was calculated through Eq. (1),

$$\text{CHO (mmol/g)} = C(V_2 - V_1)/m \tag{1}$$

where, V_1 is the amount of sodium hydroxide for DANC titration, mL; V_2 is the amount of hydrochloric acid for control titration in mL; C is the concentration of sodium hydroxide, mol L^{-1} and m is the weight of each sample, g.

2.3. Nanocomposite microgel preparation of DANC and PVAm

The dialdehyde cellulose nanocrystals were mixed with PVAm at the mass ratio of 1:1 for reaction of 24 h. Unreacted PVAm and DANC were removed with deionized water by centrifugation. The obtained nanocomposite microgel, namely CNC–PVAm, was stored at a temperature of 5 °C as its original wet state.

2.4. Characterization

2.4.1. Elemental analysis

The percentage of carbon, hydrogen, nitrogen and sulfur of nanocellulose, PVAm and the microgel were determined with a Vario EL III Elemental Analyzer (Elementar, Germany). The quantity of each element is expressed in a percentage of dry mass.

2.4.2. FT-IR

FT-IR spectra of cellulose nanocrystals and CNC–PVAm were conducted on an IRPrestige-21 Fourier Transform Infrared Spectrometer (Shimadzu Company, Japan). The samples were freeze-dried before preparing the KBr tablets. The spectra were recorded with width ranging from 400 to 4000 cm^{-1}, and resolution of 2 cm^{-1}.

2.4.3. X-ray diffraction analysis

X-ray diffraction analyses were performed with a D8 Powder X-ray Diffractometer (Bruker AXS, Germany), which was equipped with a CuXa X-ray tube. The crystallinity index (CrI) was calculated based on the Eq. (2) below (Segal et al., 1959),

$$\text{CrI} = (I_{002} - I_{am})/I_{002} \tag{2}$$

where, CrI is the crystallinity index; I_{002} is the intensity of the crystalline peak at the maximum at 2θ between 22° and 23° for cellulose I, and I_{am} is the intensity at minimum at 2θ between 18° and 19° for cellulose I.

Table 1
Information of the dyes.

Dyes	Chemical structure	λ_{max} (nm)	Charge on surface
Acid red GR		508	–
Congo red 4BS		497	–
Reactive light yellow K-4G		420	–
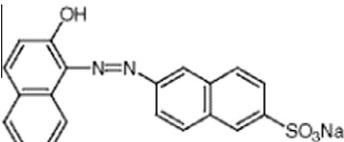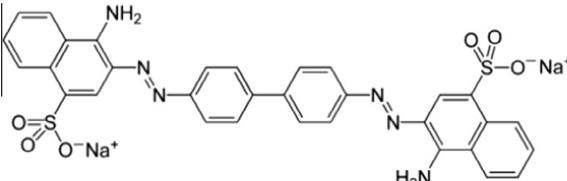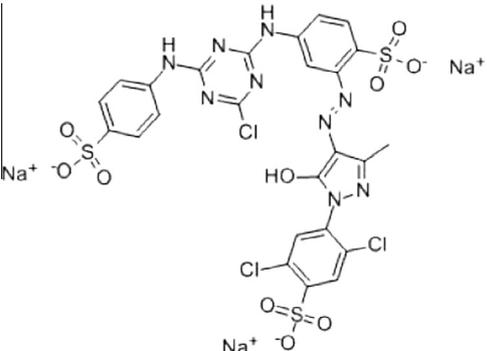
2.4.4. AFM

A Mutimode 8 Nanoscope V System AFM (Bruker Corporation, Germany) was used to observe the surface morphology of CNC, DANC and CNC–PVAm samples. A drop of dilute suspension was deposited onto a clean mica surface and air dried overnight at ambient conditions. Images from several different places on the samples were scanned.

2.4.5. Zeta potential measurement

Zeta potential of PVAm and CNC–PVAm microgel samples at various pH were determined using a Malvern Zetasizer Nano ZS90. The measurement temperature was set at 25.0 ± 0.1 °C, and the data was processed by Malvern Zetasizer Software.

2.4.6. Swelling ratio

The swelling ratios of microgel were measured at room temperature with varying pHs from 3 to 10 according to the method of Kang et al. (2012). 0.2 g of microgel was put into 20 ml of buffer solution and gently stirred for 5 h to get the equilibrium swelling. The microgel was then retrieved by a centrifugation method. The swollen microgel was weighed and the swelling ratios were determined according to the following equation,

$$\text{Swelling ratio } (\%) = (\text{wet weight} - \text{dry weight})/\text{dry weight} \times 100 \tag{3}$$

2.5. Adsorption of anionic dyes

The freeze dried microgel was mixed with dye solution and continuously stirred at 180 rpm. Samples were withdrawn at periodic time intervals from the reaction mixture. The microgel adsorbed with dyes was then removed by centrifugation at 4000 rpm for 5 min. The adsorption of the supernatant was measured using a UV–Visible spectrometer (8453, Angilent). The residual dye

concentration could be obtained using a standard curve derived from a series of dye solutions with known dye content. The adsorbed amount of dyes was calculated according to the following Eq. (4),

$$q_t = (C_0 - C_t)V/m \tag{4}$$

where, q_t is the adsorbed amount after time t, C_0 and C_t are initial concentration and concentration of the adsorbate after time t, respectively, mg L^{-1}; V is the volume of the solution, L, and m is the weight of the CNC–PVAm used, g.

The percentage removal of the dye was calculated using the following Eq. (5),

$$\% \text{ Removal} = (C_0 - C_t)/C_0 \times 100 \tag{5}$$

The study of pH influence was performed by varying the pH between 3 and 9.

3. Results and discussions

3.1. Characterization of CNC–PVAm nanocomposite microgel

Cellulose nanocrystals, extracted from fully bleached hardwood kraft pulp by sulfuric acid hydrolysis, was oxidized by sodium periodate to yield the corresponding C-2/C-3 dialdehyde nanocellulose (DANC) with an aldehyde group content of 8.81 mmol/g. The oxidized nanocrystals were then used as a crosslinker to react with PVAm to obtain CNC–PVAm microgel through a Schiff base reaction.

3.1.1. FT-IR analysis

Compared with the FT-IR spectra of unmodified CNC, a new band at around 1731 cm^{-1}, corresponding to the C=O stretching vibration of the dialdehyde cellulose nanowhisker, appeared in the spectrum of DANC. An apparent absorption peak at 883 cm^{-1} caused by the formation of hemiacetal bonds between newly achieved aldehyde groups and their neighboring hydroxyl groups

was also observed. The result indicated that the hydroxyl groups on the molecular chain of CNC were partially oxidized to aldehyde groups, obtaining the dialdehyde nanocellulose. In the spectra of PVAm, 3425 cm^{-1} and 3244 cm^{-1} corresponded to the two characteristic bands of N—H of primary amine, and 1593 cm^{-1} was N—H bending vibration, while 1673 cm^{-1} was the symmetric carboxylate stretching band, which confirmed the amphoteric structure of PVAm. FT-IR spectra of CNC–PVAm nanocomposite gave a new adsorption band at 1640 cm^{-1}, which corresponded to the stretching vibration of the Schiff base (C═N), meanwhile, the absorption band at 1731 cm^{-1} disappeared. These results supported the successful reaction of DANC with PVAm. It should be noted that the two characteristic bands in the region of 3300 cm^{-1} typical for N—H of free amines were absent for the nanocomposite, which may be attributed to the hydrogen bonding between almost all of the NH$_2$ groups and the nearby attached hydrogen atoms (Metwalli et al., 2006).

3.1.2. Elemental analysis

Table 2 lists the atomic composition of nanocellulose, PVAm and the microgel. Compared with CNC and DANC, which did not have any nitrogen, the presence of nitrogen in the microgel indicated the incorporation of PVAm. The percentage of DANC and PVAm in the microgel could be determined by comparing the nitrogen content of the microgel with that of PVAm. The result indicated that the microgel was composed of 76.7% PVAm and 23.3% nanowhiskers, respectively. The amino and carboxyl group content of PVAm could be calculated by N and O percentage (6.73 mmol/g and 8.6 mmol/g, respectively). In theory, one molecular aldehyde group can react with one molecular amino group. Thus, the free amino group content of the obtained microgel was 4.68 mmol/g, which was higher than those of nanocellulose modified by low molecular weight amines (Hokkanen et al., 2014a; Jin et al., 2015), due to the high primary amino group content of PVAm. The oxygen content of DANC was higher than that of CNC, which supports the FTIR analysis for a successful periodate oxidation. Small amounts of sulfur (0.1–0.2%) were detected in CNC, DANC and the microgel samples, resulting from the sulfate groups during the sulfuric acid hydrolysis of bleached kraft pulp. This trace amounts of sulfate groups on the surface of nanowhiskers may have a minimal effect on surface reactions (Zoppe et al., 2010).

3.1.3. XRD analysis

The X-ray diffractograms of CNC and DANC show diffraction peaks at $2\theta = 14$–18°, 22.5°, and 34.5°, which were characteristic of crystal structure of cellulose I. The cellulose I crystal structure was remained after the periodate oxidation, while the crystallinity index was reduced from 63.0% to 56.3%. It agreed well with the results of Lindh et al. (2014), who prepared 2,3-dialdehyde cellulose beads via periodate oxidation. For CNC–PVAm, the crystallinity was almost completely lost, due to the introduction of PVAm onto the oxidized nanowhiskers. Silva et al. (2013) also found an almost complete crystallinity loss of cellulose modified

with aminoethanethiol, which was ascribed to the disorder prompted by the introduction of aminoethanethiol.

3.1.4. AFM analysis

Surface morphology of the CNC, DANC and the CNC–PVAm nanocomposite were characterized by AFM. It was observed that both CNC and DANC were rod-like nanowhiskers with high aspect ratio, and the oxidation did not significantly affect the surface morphology characteristic. The width of nanowhiskers was slightly decreased after the oxidation. This was consistent with the result of Sun et al. (2015), who also found that the diameter of periodate oxidized fibers became smaller than that of the original fibers. However, Surface morphology of the microgel was completely different from that of nanowhiskers. CNC–PVAm nanocomposite was microspherical particles with a diameter ranging from 200 to 300 nm, which further confirmed the successful crosslinkage between dialdehyde nanocellulose and PVAm.

3.1.5. Zeta potential and swelling ratio

Zeta potential and swelling ratio for PVAm and CNC–PVAm at various pH are demonstrated in Fig. 1. The zeta potential was positive at low pH and negative at high pH for both samples, due to their amphoteric nature. The nanocomposite microgel possesses cationic (amino) and anionic (carboxyl and sulfate) ionizable surface groups. Its zeta potential was positive at low pH due to the protonation of amines. With the increase of the pH value, the zeta potential decreased and became negative, resulting from the deprotonation of amine groups and dissociation of carboxyl and sulfate groups on the surface. The isoelectric point (pH$_{pzc}$) for PVAm and the nanocomposite were found to be 6.4 and 5.6, respectively. Compared to that of PVAm, the isoelectric point for the nanocomposite was shifted towards lower pH, which probably was caused by the decrease of the amino groups. The result was consistent with that of Hokkanen et al. (2014a), who found the isoelectric point of aminopropyltriethoxysilane (APS) modified microfibrillated cellulose (MFC) was about 5.65.
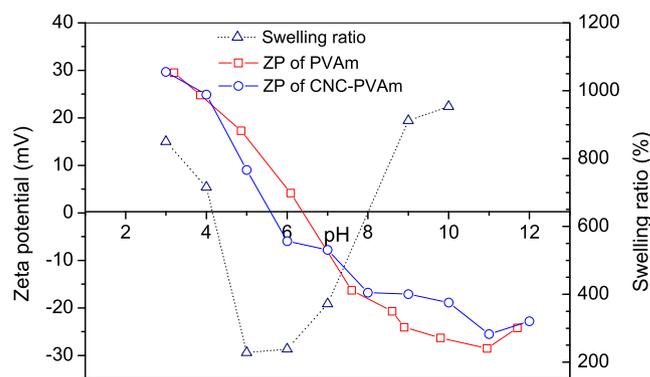

Fig. 1. Zeta potential and swelling ratio of CNC–PVAm at various pH.

Table 2
Elemental analysis of nanocellulose, PVAm and the microgel.

Sample	Content of amine groups (mmol/g)	Content of carboxyl groups (mmol/g)	Elemental composition (%)				
			C	O[a]	N	H	S
CNC			39.43	53.92		6.43	0.22
DANC			37.66	56.28		5.87	0.19
PVAm	6.73	8.6	44.64	39.05	10.10	6.21	
CNC–PVAm	4.68[b]		42.95	43.13	7.75	6.06	0.11

[a] O% = 100% − (%C + %H + %S + %N).
[b] Free amino group content % = 6.73% − 8.81 × 23.3%.
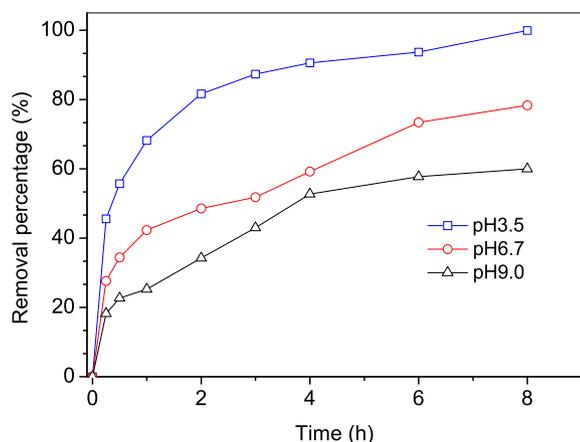
Fig. 2. Effect of initial solution pH on acid red GR removal (dye conc. = 100 mg L^{-1}; adsorbent dosage = 0.5 g L^{-1}).
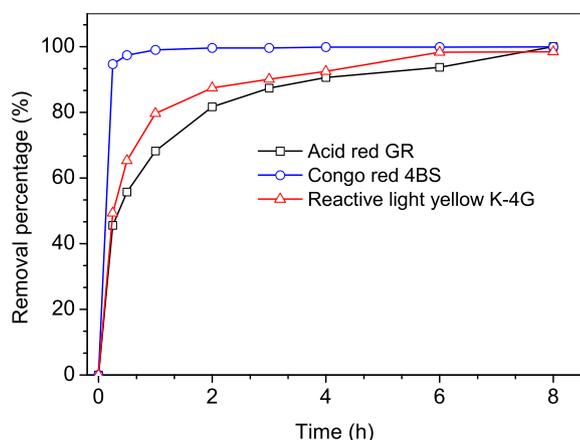

Fig. 3. Percentage removal of different anionic dyes using ANCC (dye conc. = 100 mg L^{-1}; adsorbent dosage = 0.5 g L^{-1}).

The swelling ratio also exhibited a corresponding pH dependency as the zeta potential. It is well known that the swelling of hydrogel is induced by the electrostatic repulsion of the ionic charges of its network (Karadağ et al., 2002). Under an acidic condition, the protonation of amino groups would develop an electrostatic repulsion, resulting in the swelling of the microgel. With the increasing of the pH, the deprotonation of amino groups mitigated the repulsion, so the microgel would de-swell. However, when the pH was higher than the isoelectric point, the swelling ratio increased due to the deprotonation of carboxyl groups.

3.2. Adsorption of anionic dyes

3.2.1. pH effect on removal percentage

pH is one of the most important process variables when considering dye adsorption. As has been reported (Ibrahim et al., 2010), the adsorption of a positive charged adsorbate is favored when the pH of the solution is greater than the pH$_{pzc}$ of the adsorbent, whereas the adsorption of negatives charges, in turn, is favored at pH levels less than pH$_{pzc}$. Therefore, the adsorption of the anionic dyes is expected to be favored in solution with pH values less than the pH$_{pzc}$ of the adsorbent. During the dying process, acetic acid is often used as a stimulator, in which the dye solution pH is normally adjusted from 3 to 4. It is desirable that the adsorbent demonstrates its maximum capacity at this pH range, without the necessity of adjusting pH during the adsorption process. In this study, CNC–PVAm microgel was used as an adsorbent to remove the acid red GR in the aqueous solution at a pH range of 3.5–9.0, as shown in Fig. 2. It is obvious that at pH 3.5, the removal percentage of dye was 99.9% (q_t = 199.8 mg g^{-1}), higher than 78.3% (q_t = 156.7 mg g^{-1}) in the neutral region (pH 6.7) and 59.9% (q_t = 119.9 mg g^{-1}) at pH 9. This could be attributed to zeta potential changes in surface electric charge of the CNC–PVAm microgel. Various functional groups such as amine, hydroxyl and carboxyl groups distributed on the surface of the microgel. Lower pH led to more amine groups protonation (NH$_3^+$) of the microgel, resulting in more positive charges on the surface. The anionic dye removal could be enhanced by strong electrostatic attraction between the protonated amine and negatively charged SO$_3^{2-}$ groups of dye. As pH increased, deprotonation of amino groups started and the reduction of electrostatic attraction resulted in the decrease in adsorption capacity. Moreover, the deprotonation of carboxyl groups (COO$^-$) enhanced the electric repulsion between the anionic dyes and the microgel, limiting the chemical interaction between CNC–PVAm surface and the anionic site of the dye, which further decreases the adsorption capacity. At alkaline pH, the interaction on the surface of dye and microgel is hydrogen bonding.

3.2.2. Adsorption kinetics

Dyes are usually classified based on their particle charge upon dissolution in aqueous application medium (Yagub et al., 2014), such as cationic (all basic dyes), anionic (direct, acid, and reactive dyes), and non-ionic (dispersed dyes). The removal efficiency of different anionic dyes, congo red 4BS (direct dye), acid red GR (acid dye) and reactive light yellow K-4G (reactive dye) using CNC–PVAm versus time are shown in Fig. 3. It was noted that the adsorption equilibrium for congo red 4BS was achieved within 1 h, much quicker compared to the acid and reactive dyes, which achieved equilibrium using about 8 h. The removal efficiency of the three dyes all reached almost 100% at adsorption equilibrium, which demonstrated that the nanocomposite microgel can be utilized for the adsorption of different anionic dyes at a low dosage.

Table 3
Pseudo first and second order parameters for the adsorption.

	Dyes	Acid red GR	Congo red 4BS	Reactive light yellow K-4G
First order	k_1 (h^{-1})	0.3796	0.6648	0.8733
	$q_{e\ cal}$ (mg g^{-1})	96.1	5.4	126.4
	R^2	0.935	0.808	0.882
Second order	k_2 (g mg^{-1} h^{-1})	0.00137	0.517	0.0209
	$q_{e\ cal}$ (mg g^{-1})	202.8	200.0	201.2
	R^2	0.995	1.000	0.998
Intraparticle diffusion	k_{id} (mg g^{-1} h$^{-0.5}$)	44.67	3.46	37.7
	c	85.2	191.9	105.7
	R^2	0.891	0.540	0.790
$q_{e\ exp}$ (mg g^{-1})		199.9	199.8	196.9

The adsorption kinetics illustrates the dye adsorption rate and eventually explores the mechanism of adsorption and the rate limiting steps involved. To investigate the adsorption process of anionic dyes on the nanocomposite microgel, the pseudo first-order, pseudo second-order, and intraparticle diffusion models were used to fit the experimental results. The equations are expressed as follows,

First order kinetic model : $\log(q_e - q_t) = \log q_e - k_1 t/2.303$ (6)

Second order kinetic model : $t/q_t = 1/(k_2 q_e^2) + t/q_e$ (7)

Intraparticle diffusion model : $q_t = k_{id}t^{0.5} + c$ (8)

where, q_e and q_t are the amount of adsorbed dye per unit mass of adsorbent (mg g^{-1}) at equilibrium and at time t, respectively; k_1 is the pseudo first order sorption rate constant (h^{-1}); k_2 is the rate constant of pseudo second order adsorption (g mg^{-1} h^{-1}); k_{id} is the rate constant of intraparticle diffusion (mg g^{-1} h$^{-0.5}$), and c indicates the thickness of boundary layer.

The kinetic parameters were calculated accordingly and listed in Table 3. The correlation coefficients for the second order model were all greater than 0.99 for the three dyes, while those for the first order model were between 0.808–0.935, and 0.540–0.891 for the intraparticle model. The values of R^2 fitted by intraparticle diffusion model were not very high, indicating that intraparticle diffusion was not the rate-limiting step in the adsorption process. From R^2 of various kinetics models, pseudo second order model was more suitable to describe the adsorption kinetics behaviors. Moreover, the equilibrium adsorption values calculated by the second order model ($q_{e\ cal}$) matched well with experimental adsorption results ($q_{e\ exp}$), which further confirmed that the kinetics of adsorption by CNC–PVAm for the three anionic dyes was best described by the pseudo second order model. This indicated that the rate controlling mechanism for adsorption was chemisorption. Second order kinetics of dye adsorption was also observed for some biosorbents (Ghorai et al., 2013; Nair et al., 2014; Roy et al., 2012). It should also be noted that the rate constant k_2, for the adsorption of congo red (0.517), was much higher than those for acid red and reactive light yellow (0.0137 and 0.0209, respectively), which confirms the higher adsorption rate of CNC–PVAm microgel for congo red 4BS.

3.2.3. Adsorption isotherms

The equilibrium adsorption isotherm is also used to understand the mechanism of the adsorption. Adsorption isotherm models describe the interaction between the adsorbate and adsorbent. In this work, classic isotherm models, Langmuir, Freundlich and Sips were used to obtain the isotherm parameters for adsorption of dyes onto CNC–PVAm. The Langmuir isotherm model is based on a monolayer adsorption onto a surface with a finite number of adsorption sites of uniform adsorption energies. It can be expressed as the following equation,

$$q_e = q_m K_L C_e/1 + K_L C_e \quad (9)$$

where, q_e is the equilibrium adsorption capacity, mg g^{-1}; C_e is the equilibrium concentration of adsorbate in the solution, mg L^{-1}; q_m is the maximum amount of the dyes adsorbed per unit weight of the adsorbent, which also describes the formation of complete monolayer coverage on the surface at high equilibrium concentration of dyes, mg g^{-1}; K_L is the Langmuir adsorption equilibrium constant related to the affinity of the binding sites and indicates the bond energy of the adsorption reaction between adsorbent and adsorbate, L g^{-1}.

The Freundlich isotherm model is an empirical equation, which is utilized to understand adsorption on heterogeneous surfaces
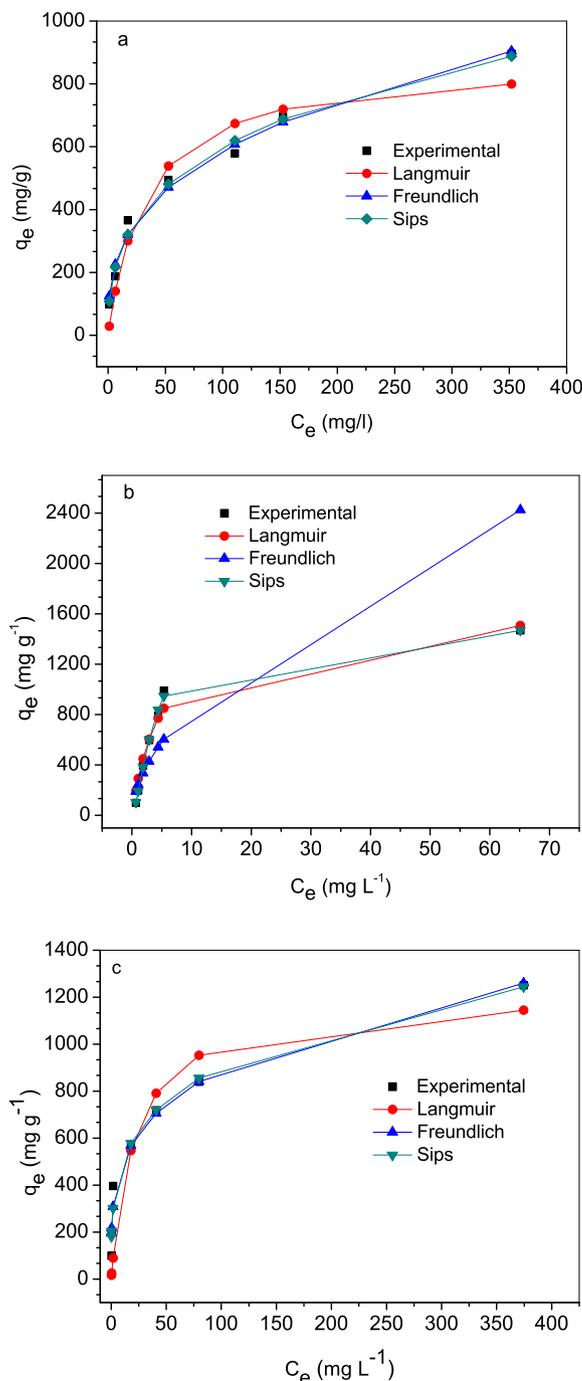

Fig. 4. Various adsorption isotherms fit by CNC–PVAm, (a) acid red GR; (b) congo red 4BS; (c) reactive light yellow K-4G (adsorbent dosage = 0.5 g L^{-1}).

with multiple adsorption layers (Kyzas et al., 2014). It can be expressed as the following equation,

$$q_e = K_F C_e^{1/n} \quad (10)$$

where, K_F (mg g^{-1}) and n are Freundlich constants related to the adsorption capacity and adsorption intensity and spontaneity, respectively. The value of n in the range of $1 < n < 10$ indicates a favorable adsorption process. The greater the value of n, the better is the favorability of the adsorption.

The Sips model is a combination of Langmuir and Freundlich isotherms (Hokkanen et al., 2014b), which takes the following form:

Table 4
Langmuir, Freundlich and Sips isotherms parameters for the adsorption.

Dyes		Acid red GR	Congo red 4BS	Reactive light yellow K–4G
Langmuir	q_m (mg g^{-1})	873.8	1619.9	1210.6
	K_L (L g^{-1})	0.0305	0.210	0.0462
	R^2	0.92	0.96	0.80
Freundlich	K_F (mg g^{-1})	120.3	267.3	237.1
	n	2.91	1.78	3.82
	R^2	0.985	0.770	0.974
Sips	q_s	877.3	1491.6	1152.6
	K_S (mL mg^{-1})	0.039	0.130	0.053
	m	0.426	1.520	0.310
	R^2	0.984	0.995	0.978
$q_{e\ exp}$ (mg/g)		896.1	1469.7	1250.9

Table 5
Comparison of adsorption capacity of anionic dyes by some cellulose-based adsorbents.

Adsorbent	Dye	q_e (mg/g)	Reference
Nanocellulose hybrid	Reactive blue B-RN	14	Xie et al. (2011)
	Reactive yellow B-4RFN	16	
Modified straw	Methyl orange	300	Zhang et al. (2012)
	Acid green	950	
Modified walnut shell	Reactive brilliant red K-2BP	568	Cao et al. (2014)
Cellulose modified with aminoethanethiol	Reactive red RB	78	Silva et al. (2013)
Quaternized cellulose nanofibrils nanocellulose	Acid green 25	683	Pei et al. (2013)
	Congo red	664	
Partially hydrolyzed polyacrylamide/cellulose nanocrystal hydrogel	Methylene blue	326	Zhou et al. (2014)
CNC–PVAm	Acid red GR	896	This work
	Congo red 4BS	1469	
	Reactive light yellow K-4G	1250	

$$q_e = q_s K_S C_e m / 1 + K_S C_e m \tag{11}$$

where, q_s is the specific adsorption capacity at saturation, mg g^{-1}; K_S is Sips isotherm constant related to energy of adsorption, mL mg^{-1}, and m is the heterogeneity factor. If the value of K_S approaches to zero, Sips isotherm equation follows the Freundlich isotherm model, while the value of m equal or close to 1, the Sips isotherm equation reduced to the Langmuir isotherm.

The plots of the adsorption isotherms are illustrated in Fig. 4 and the calculated parameters are listed in Table 4. It was found that for all the three dyes, Sips model gave the best description of the adsorption, with $R^2 > 0.97$. q_s value estimated by the Sips model corresponded well with the $q_{m\ exp}$. For acid red and reactive light yellow, Freundlich isotherm model also described the adsorption accurately. The values of "n" were in the range of $1 < n < 10$, indicating a favorable adsorption process. K_S value was 0.039 and 0.053, respectively, which was very small. In this case, Sips isotherm equation follows the Freundlich isotherm model, indicating a heterogeneous multilayer adsorption process. For congo red, the adsorption fitted the best with the Sips model, with an R^2 of 0.995. Compared to the other two dyes, the nanocomposite demonstrated the highest adsorption capacity for congo red. A similar trend was observed by Wawrzkiewicz et al. (2015), who investigated the adsorptive removal of anionic dyes using mixed silica-alumina oxide and found that the affinity series of the dyes for oxide could be presented as, C. I. Direct Blue 71 > C. I. Reactive Black 5 > C. I. Acid Orange 7. Variations in K_L values of dyes indicated the difference of adsorption energies between the adsorbent and dyes. High K_L value of congo red related to very fast adsorption, which was consistent with the results of the kinetic study.

A comparison of the adsorption capacity of CNC–PVAm to some cellulose-based adsorbents is presented in Table 5. It can be seen that CNC–PVAm has a relatively high adsorption capacity for the anionic dyes, indicating a significant potential for the removal of these dyes from aqueous solutions.

4. Conclusions

Nanocomposite microgel, based on dialdehyde nanocellulose and amphoteric PVAm, has been found to be an excellent adsorbent for removal of anionic dyes. It demonstrated the maximum removal efficiency at acidic conditions due to the protonation of amino groups. The nanocomposite microgel can be utilized for the adsorption of different types of anionic dyes and showed the highest adsorption capacity for congo red. The adsorption of the anionic dyes onto the microgel followed pseudo second order kinetics, indicating that dye adsorption was mainly controlled by chemisorption behavior. The adsorption isotherms of the microgel could be well described by Sips model.

Appendix A. Supplementary data

Supplementary data associated with this article can be found, in the online version, at http://dx.doi.org/10.1016/j.biortech.2015.08.093.

References

Bonetto, L.R., Ferrarini, F., Marco, C..De., Crespo, J.S., Guégan, R., Giovanela, M., 2015. Removal of methyl violet 2B dye from aqueous solution using a magnetic composite as an adsorbent. J. Water Proc. Eng. 6, 11–20.

Cao, J.S., Lin, J.X., Fang, F., Zhang, M.T., Hu, Z.R., 2014. A new absorbent by modifying walnut shell for the removal of anionic dye: kinetic and thermodynamic studies. Bioresour. Technol. 163, 199–205.

Ghorai, S., Sarkar, A.K., Panda, A.B., Pal, S., 2013. Effective removal of Congo red dye from aqueous solution using modified xanthan gum/silica hybrid nanocomposite as adsorbent. Bioresour. Technol. 144, 485–491.

Hokkanen, S., Repo, E., Suopajarvi, T., Liimatainen, H., Niinimaa, J., Sillanpaa, M., 2014a. Adsorption of Ni(II), Cu(II) and Cd(II) from aqueous solutions by amino modified nanostructured microfibrillated cellulose. Cellulose 21, 1471–1487.

Hokkanen, S., Repo, E., Westholm, L.J., Lou, S., Sainio, T., Sillanp, M., 2014b. Adsorption of Ni^{2+}, Cd^{2+}, PO_4^{3-} and NO_3^- from aqueous solutions by nanostructured microfibrillated cellulose modified with carbonated hydroxyapatite. Chem. Eng. J. 252, 64–74.

Ibrahim, S., Fatimah, I., Ang, H.M., Wang, S.B., 2010. Adsorption of anionic dyes in aqueous solution using chemically modified barley straw. Water Sci. Technol. 62, 1177–1182.

Jebali, A., Behzadi, A., Rezapor, I., Jasemizad, T., Hekmatimoghaddam, S.H., Halvani, Gh.H., Sedighi, N., 2015. Adsorption of humic acid by amine-modified nanocellulose: an experimental and simulation study. Int. J. Environ. Sci. Technol. 12, 45–52.

Jin, L.Q., Li, W.G., Xu, Q.H., Sun, Q.C., 2015. Amino-functionalized nanocrystalline cellulose as an adsorbent for anionic dyes. Cellulose 22, 2443–2456.

Kang, M.K., Hong, S.K., Seo, Y.C., Kim, Y.O., Lee, H.Y., Kim, J.C., 2012. Chitosan microgel: effect of cross-linking density on pH-dependent release. Korean J. Chem. Eng. 29, 72–76.

Karadağ, E., Üzüm, Ö.B., Saraydin, D., 2002. Swelling equilibria and dye adsorption studies of chemically crosslinked superabsorbent acrylamide/maleic acid hydrogels. Euro. Polym. J. 2002 (38), 2133–2141.

Kayranli, B., 2011. Adsorption of textile dyes onto iron based waterworks sludge from aqueous solution: isotherm, kinetic and thermodynamic study. Chem. Eng. J. 173, 782–791.

Kyzas, G.Z., Lazaridis, N.K., Kostoglou, M., 2014. Adsorption/desorption of a dye by a chitosan derivative: experiments and phenomenological modeling. Chem. Eng. J. 248, 327–336.

Lindh, J., Carlsson, D.O., Strømme, M., Mihranyan, A., 2014. Convenient one-pot formation of 2,3-dialdehyde cellulose beads via periodate oxidation of cellulose in water. Biomacromolecules 15, 1928–1932.

Liu, P., Sehaqui, H., Tingaut, P., Wichser, A., Oksman, K., Mathew, A.P., 2014. Biobased nanomaterials for capturing silver ions (Ag^+) from water via surface adsorption. Cellulose 21, 449–461.

Maatar, W., Alila, S., Boufi, S., 2013. Cellulose based organogel as an adsorbent for dissolved organic compounds. Ind. Crops Prod. 49, 33–42.

Metwalli, E., Haines, D., Becker, O., Conzone, S., Pantano, C.G.C., 2006. Surface characterizations of mono-, di-, and triaminosilane treated glass substrates. J. Colloid Interface Sci. 298, 825–831.

Nair, V., Panigrahy, A., Vinu, R., 2014. Development of novel chitosan-lignin composites for adsorption of dyes and metal ions from wastewater. Chem. Eng. J. 254, 491–502.

Ong, S.T., Lee, C.K., Zainal, Z., 2007. Removal of basic and reactive dyes using ethylenediamine modified rice hull. Bioresour. Technol. 98, 2792–2799.

Pei, A., Butchosa, N., Berglund, L.A., Zhou, Q., 2013. Surface quaternized cellulose nanofibrils with high water absorbency and adsorption capacity for anionic dyes. Soft Matter 9, 2047–2055.

Pelton, R., 2014. Polyvinylamine: a tool for engineering interfaces. Langmuir 30, 15373–15382.

Qu, X., Alvarez, P.J.J., Li, Q., 2013. Applications of nanotechnology in water and wastewater treatment. Water Res. 47, 3931–3946.

Roy, A., Chakraborty, S., Kundu, S.P., Adhikari, B., Majumder, S.B., 2012. Adsorption of anionic-azo dye from aqueous solution by lignocellulose biomass jute fiber: equilibrium, kinetics, and thermodynamics study. Ind. Eng. Chem. Res. 51, 12095–12106.

Savage, N., Diallo, M.S., 2005. Nanomaterials and water purification: opportunities and challenges. J. Nanomater. Res. 7, 331–342.

Segal, L., Creely, J.J., Martin Jr., A.E., Conrad, C.M., 1959. An empirical method for estimating the degree of crystallinity of native cellulose using X-ray diffractometer. Text. Res. J. 29, 786–794.

Silva, L.S., Lima, L.C.B., Silva, F.C., Matos, J.M.E., Santos, M.R.M.C., Santos Jr., L.S., 2013. Dye anionic sorption in aqueous solution onto a cellulose surface chemically modified with aminoethanethiol. Chem. Eng. J. 218, 89–98.

Sun, B., Hou, Q.X., Liu, Z.H., Ni, Y.H., 2015. Sodium periodate oxidation of cellulose nanocrystal and its application as a paper wet strength additive. Cellulose 22, 1135–1146.

Unuabonah, E.I., Taubert, A., 2014. Clay-polymer nanocomposites (CPNs): adsorbents of the future for water treatment. Appl. Clay Sci. 99, 83–92.

Wang, Y., Mu, Y., Zhao, Q.B., Yu, H.Q., 2006. Isotherms, kinetics and thermodynamics of dye biosorption by anaerobic sludge. Sep. Purif. Technol. 50, 1–7.

Wawrzkiewicz, M., Wisniewska, M., Gunko, V.M., Zarko, V., 2015. Adsorptive removal of acid, reactive and direct dyes from aqueous solutions and waste water using mixed silica-alumina oxide. Powder Technol. 278, 306–315.

Xie, K.L., Zhao, W.G., He, X.M., 2011. Adsorption properties of nano-cellulose hybrid containing polyhedral oligomeric silsesquioxane and removal of reactive dyes from aqueous solutions. Carbohydr. Polym. 83, 1516–1520.

Yagub, M.T., Sen, T.K., Afroze, S., Ang, H.M., 2014. Dye and its removal from aqueous solution by adsorption: a review. Adv. Colloid Interface Sci. 209, 172–184.

Zhang, W.X., Li, H.J., Kan, X.W., Dong, L., Yan, H., Jiang, Z.W., Yang, H., Li, A.M., Cheng, R.S., 2012. Adsorption of anionic dyes from aqueous solutions using chemically modified straw. Bioresour. Technol. 117, 40–47.

Zhou, C.J., Wu, Q.L., Lei, T.Z., Negulescu, I.I., 2014. Adsorption kinetic and equilibrium studies for methylene blue dye by partially hydrolyzed polyacrylamide/cellulose nanocrystal nanocomposite hydrogels. Chem. Eng. J. 251, 17–24.

Zoppe, J.O., Habibi, Y., Rojas, O.J., Venditti, R.A., Johansson, L.S., Efimenko, K., Osterberg, M., Laine, J., 2010. Poly(N-isopropylacrylamide) brushes grafted from cellulose nanocrystals via surface-initiated single-electron transfer living radical polymerization. Biomacromolecules 11, 2683–2691.